CORA Cork Open Research Archive
Cartlann Taighde Oscailte Chorcaí

Title	Spatial distribution of glucose and amino acids within all-aqueous emulsions directs the Maillard reaction and oxidation pathways
Authors	Chen, Kangni;Madadlou, Ashkan;De Pascale, Sabrina;Scaloni, Andrea;Fogliano, Vincenzo;Troise, Antonio Dario
Publication date	2026-03-21
Original Citation	Chen, K, Madadlou, A, De Pascale, S, Scaloni, A, Fogliano, V & Troise, A D 2026, 'Spatial distribution of glucose and amino acids within all-aqueous emulsions directs the Maillard reaction and oxidation pathways', Communications Chemistry, vol. 9, no. 1, 176, pp. 1-14. https://doi.org/10.1038/s42004-026-01951-6
Type of publication	Article (peer-reviewed)
Link to publisher's version	https://www.scopus.com/pages/publications/105038591800 - 10.1038/s42004-026-01951-6
Rights	© 2026, the Author(s). This article is licensed under a Creative Commons Attribution-NonCommercial-NoDerivatives 4.0 International License, which permits any non-commercial use, sharing, distribution and reproduction in any medium or format, as long as you give appropriate credit to the original author(s) and the source, provide a link to the Creative Commons licence, and indicate if you modified the licensed material. - https://creativecommons.org/licenses/by-nc-nd/4.0/
Download date	2026-11-17 04:27:42
Item downloaded from	https://hdl.handle.net/10468/19239

UCC
University College Cork, Ireland
Coláiste na hOllscoile Corcaigh

communications chemistry

Article

A Nature Portfolio journal

https://doi.org/10.1038/s42004-026-01951-6

Spatial distribution of glucose and amino acids within all-aqueous emulsions directs the Maillard reaction and oxidation pathways

Check for updates

Kangni Chen[1], Ashkan Madadlou[2], Sabrina De Pascale[3], Andrea Scaloni[3], Vincenzo Fogliano[1] & Antonio Dario Troise[3]

All-aqueous emulsions represent a versatile platform for studying and controlling chemical reactions in foods and biological systems. Through the compartmentalization and segregation of reactants, distinct molecularly crowded microenvironments enable the generation of unique reaction products. We explored how spatial organization within all-aqueous emulsions composed of polyethylene glycol (PEG) and sodium sulfate (Na_2SO_4) modulates the Maillard reaction and oxidation reactions between glucose and amino acids. Using untargeted metabolomics and molecular networking, we characterized the chemical diversity of reaction products formed when the reactants were either co-encapsulated within the droplet phase or distributed (segregated) between the two phases of the emulsions. Over 500 compounds were annotated across both systems, revealing distinct molecular profiles driven by reactant localization and phase partitioning. When the precursors were segregated (tryptophan and glucose), oxidation products as aminobenzoyl-, hydroxy- and hydroperoxy-derivatives accumulated preferentially in the PEG phase. Conversely, when the reactants were co-encapsulated (asparagine and glucose) within Na_2SO_4 droplets, enhanced formation of the Amadori products and dipeptides was observed, guided by phase-specific microenvironment. Our results demonstrate that the reactant location, in addition to time and temperature, plays a critical role in modulating food-relevant reactions, with a new framework for controlling the formation of glycation compounds via emulsion-based microreactors.

Droplet reactors, particularly those based on all-aqueous (water-in-water, W/W) emulsions, have emerged as versatile platforms for carrying out chemical reactions within molecularly crowded biphasic systems[1]. The physicochemical properties of all-aqueous emulsions influence the location of reactants (precursors), directing specific chemical reactions to occur either within the dispersed droplets (i.e., compartmentalized), at the interface between the two phases or in the continuous bulk phase. Chemical reactions that can be studied using such droplet-based systems include hydrolysis, as well as acid-base, redox and enzymatic reactions. Each of these is influenced by the chemical nature of the reactants and by the tendency of precursors to partition between the two aqueous phases or accumulate at the interface[2].

Among the many chemical transformations that can occur in such biphasic systems, the Maillard reaction (MR) is of particular interest due to its complexity and importance in food chemistry. The MR produces a wide variety of volatile and non-volatile compounds. Volatile products include sulfur-, nitrogen- and oxygen-containing heterocycles (e.g., pyrazines, thiazoles, furans), as well as Strecker aldehydes[3–5]. Non-volatile products range from early-stage compounds, like Amadori products, to melanoidins and advanced glycation end-products[6,7]. It is known that their

[1]Food Quality and Design Group, Wageningen University & Research, Wageningen, The Netherlands. [2]School of Food and Nutritional Sciences, University College Cork (UCC), Cork, Ireland. [3]Proteomics, Metabolomics & Mass Spectrometry Laboratory, ISPAAM, National Research Council, Portici, Italy.
e-mail: antoniodario.troise@cnr.it

formation depends on factors such as precursor type, temperature, pH, and water activity[8].

However, much less is understood about how the spatial localization, intended as the distribution and dynamics of reactants and products within multiphase systems, affects reactants and products retention, concentration, and migration across phase boundaries. In foods, reactions rarely occur in chemically uniform environments; instead, they take place in systems characterized by gradients in water activity, polarity, and molecular crowding. These microenvironmental factors, often overlooked in studies performed in homogeneous aqueous solutions, can profoundly influence the Maillard and associated reactions such as Strecker degradation, dehydration, retro-aldol cleavage, condensation and oxidation[9]. Elucidating how molecular organization and phase behavior modulate these processes can provide a foundation for controlling the generation of desirable flavor and color compounds while mitigating the formation of undesirable oxidation or toxic products.

Effective analysis of diverse compounds generated during the MR in all-aqueous emulsions requires specialized analytical methods tailored to their dynamic microenvironment. Untargeted metabolomics provides a holistic profiling of the molecular species, enabling detailed characterization of both temporal (i.e., over time) and spatial (i.e., across compartments) variations in reaction intermediates and products. This systems-level approach is particularly valuable in deciphering the pathways of the MR and concomitant processes, such as oxidation, which may occur even in simple sugar–amino acid model systems. Similar strategies have been applied in studying the peroxidation of lipids and volatile compounds formation during food processing[10,11]. In the context of untargeted metabolomics for decoding the MR pathways in droplet-based reactors, the application of hydrophilic interaction liquid chromatography high-resolution mass spectrometry (HILIC-HRMS) is the technique of choice to match the hydrophilic nature of the most relevant amino and carbonyl precursors.

Our prior work demonstrated that all-aqueous emulsions can control the spatial distribution of amino acids, reducing sugars, and the corresponding reaction intermediates (i.e., the Amadori compounds), thereby subsequent pathways[12]. Although that study established the role of the emulsions in modulating early-stage reactions through compartmentalization and segregation, two unanswered questions persist: (I) how the spatial organization tackles the molecular diversity of end-products, and (II) how their formation and migration through different phases depend on amino acid partitioning behavior. Here, untargeted metabolomics and molecular networking[13] were used to annotate and possibly identify the end-products formed and to elucidate the MR and oxidation pathways in all-aqueous emulsions through multivariate data analysis.

Upon the preparation of all-aqueous emulsions, the reactants were partitioned either inside the droplets (co-encapsulation, for asparagine and glucose) or segregated between the interior and exterior phases of the emulsions (yet interfacially touching, for tryptophan and glucose) according to the amino acid side chain[12]. Glucose was selected as a carbonyl compound ubiquitous in foods and biological systems, while asparagine, owing to its high hydrophilicity, was co-encapsulated with glucose within droplets; indeed, their partition coefficients are 0.206 and 0.080, respectively. In contrast, the hydrophobic side chain tryptophan (partition coefficient 6.17) preferentially partitions into the PEG-rich phase. Its indole group further imparts distinctive reactivity, supporting the study of a broader spectrum of the MR.

The present work extends the investigation to the end-product level by employing untargeted metabolomics combined with molecular networking. This systems-level approach allows compounds annotation potentially implicated in condensation reaction along with degradation products involved in polymerization reaction. Such information can reveal how product migration and phase-specific accumulation depend on amino acid partitioning behavior and reaction microenvironment. In this way, the results advance from qualitative observation of spatial control to a semi-quantitative and mechanistic understanding of phase-driven chemical selectivity in all-aqueous droplet reactors.

Results and discussion

The analytical background for the definition of the chemical space behind reaction mechanisms in all-aqueous emulsions

The spatial distribution of reaction precursors, including amino groups and reducing sugars within all-aqueous emulsions, leads to the formation of thousands of compounds with distinct properties. We opted for zwitterionic HILIC as a flexible technique to separate polar charged compounds present in an aqueous environment. This method also guaranteed a good response for the separation of chromophores and brown pigments or polymers (usually separated in reversed phase chromatography) formed in both tryptophan- and asparagine-supplemented samples as a result of condensation, oxidation, and polymerization reactions[14]. Then, HRMS-based metabolomics provided the analytical context for the annotation and identification of unknown end-products formed[10]. Control samples and procedural blanks were used to define the chemical space in the untargeted analysis; in full scan mode, a total of 524 signals were detected in the system with segregated reactants compared to 917 signals in the system where reactants were co-encapsulated. To improve the reliability of chemical feature responses, exclusion filter criteria removed the signals that were not associated with any chemical formulas due to poor matching with theoretical isotopic pattern distribution. Next, we considered only compounds in tandem MS mode that generated a fragmentation mass spectrum and added structural information to the isotopic pattern. The third filter included a chromatographic peak score higher than 5 as the result of the profiles associated with the scan points below each peak in all the replicates (8 scans per peak as minimum). Finally, the metabolomic workflow included two separate procedures: each run was screened first in polarity switching mode by considering both ionization modalities. Annotated compounds in polarity switching experiments were further checked in reprocessing workflows with exclusive positive or negative ion mode. Wherever possible, spectra were manually curated in both positive and negative mode by excluding co-eluting compounds with overlapping peak shapes that could result from in-source ionization or fragmentation typical of analytical procedures that involve a broad ratio between the highest and lowest signal intensities[15]. Upon all the filtering procedures, we annotated 264 compounds in all the tryptophan-supplemented samples and 301 compounds in all asparagine-supplemented samples. In Supplementary Data 1 and 2, we reported for each compound an identification level ranging from 1 (compound identification upon matching to analytical standards as the amino acids and glucose as precursors and the two Amadori compounds as intermediate, reported in bold) to 2 (compounds annotation based on mass spectra, isotopic pattern, chemical formula, mass accuracy and matching with databases when compound names are present) according to Metabolomics standard initiative level[16]. In this view, we decided to keep tryptophan-supplemented and asparagine-supplemented samples separated, exploring the type of compounds formed and their reactivity[12].

Tryptophan and glucose reactivity in reactants segregation

Figure 1 provides a sample distribution overview of tryptophan-supplemented samples at time 0 and at 5 h, 95 °C in the form of a principal component analysis (PCA), accompanied by loadings plot and a molecular network of the annotated compounds. Figure 1A illustrates that the overall variance explained by the analysis was 47.8%, with the first principal component (PC1) accounting for 27.9% and the second principal component (PC2) for 19.9%. PC1 primarily captures the significant differences between the two reaction times (e.g., 0 h vs. 5 h), indicating that the reaction pathways undergo substantial changes over time. Since PC1 explains most of the variance, it underscores the dominant role of the reaction time in the sample distribution. The PEG_0 and EP_0 samples were in the fourth quadrant, while after 5 h at 95 °C, EP and PEG samples shifted to the third quadrant. Moreover, EP_5 and PEG_5 clustered together in the same region, suggesting that these samples generated similar reaction product profiles after heating. This observation indicates that EP acted as the main site for subsequent transformations, leading to similar reaction pathways and product distributions as seen in the PEG samples. On the

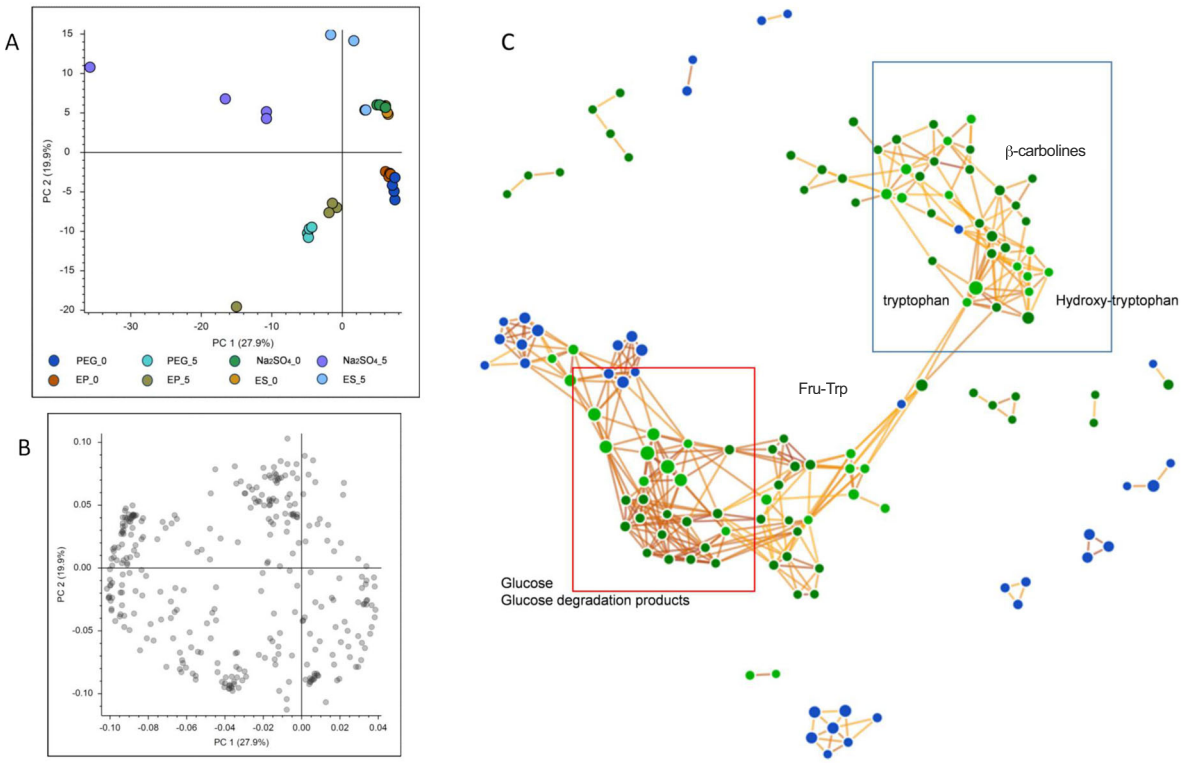

Fig. 1 | 2D sample distribution, compound loadings plot, and molecular networking upon filtering procedure of ddMS² experiments for reactants segregation reaction mode. A The principal component analysis (PCA) of the four model systems at time 0 and after 5 h at 95 °C. Colors indicate different time points and systems: EP (Emulsion PEG phase), ES (Emulsion Na_2SO_4 phase), PEG (PEG solution), and Na_2SO_4 (Na_2SO_4 solution). **B** The compound loadings plot, with dark grey indicating compound accumulation after 5 h of thermal treatment. **C** The chemical space in the form of a molecular network based on similarities between fragmentation spectra, including glucose, tryptophan and their putative degradation products, linked via the Amadori compound of tryptophan (indicated as Fru-Trp). Annotated molecules are shown in green according to their level of identification based on publicly available databases or internal mass list, whereas unknowns in blue. Yellow lines connect compounds with similar fragmentation patterns in ddMS² according to specific chemical transformations. The network was built across all four systems without using time as a grouping variable to reveal relationships among precursors, intermediates, and end-products.

other hand, PC2 highlights the significant differences between the PEG and Na_2SO_4 phases, reflecting the distinct chemical behaviors of these phases during the reaction process. The ES_0 and ES_5 samples were in the first quadrant, while EP_0 and EP_5 were in the fourth and third quadrants, respectively. The PEG phase exhibited stronger reactivity, particularly at higher temperatures, where a range of complex Maillard reaction products and tryptophan oxidation products accumulate. In contrast, the Na_2SO_4 phase remained relatively stable between 0 and 5 h, suggesting that the reaction products in this phase changed more gradually, with a predominance of glucose degradation products. This stability of the Na_2SO_4 phase in segregation mode and its lower reactivity supported the notion that the Na_2SO_4 phase primarily participated in reactant migration and partial reactions, rather than facilitating large-scale product transformations. This two-dimensional distribution corresponded to the molecular loadings shown in Fig. 1B, where each grey point represents one of the compounds annotated when reactants were segregated between the emulsion phases. As expected, dark grey datapoints predominantly clustered within the second and third quadrants (Q2-Q3), corresponding to compounds exhibiting significantly elevated response intensities in PEG_5, EP_5, and Na_2SO_4_5 samples. This pattern is likely attributed to the effects of prolonged thermal processing (95 °C for 5 h), which promoted advanced glycation and oxidation reactions, as well as cleavage and polymerization processes.

Figure 1C presents information on the molecular interrelationships of the high-resolution tandem mass spectra between compounds annotated in the glucose and tryptophan model systems. The molecular network pinpoints the overall chemical patterns independently of model system compositions, with green points representing annotated compounds and blue points indicating unknown compounds. The red box highlighted the fragmentation spectra of the degradation products associated with glucose, including putative intermediates involved in dicarbonyl formation and small organic acids. In contrast, the blue box outlined compounds with fragmentation spectra similar to those of tryptophan, such as indole derivatives, β-carbolines, while quinolines and aminobenzoyl-derivatives formed their own pattern. Glucose and tryptophan compartments were connected by *N*-(1-deoxy-D-fructos-1-yl)-tryptophan (indicated as Fru-tryptophan, the Amadori compounds arising from glucose and tryptophan), which exhibited fragmentation patterns consistent with those of glucose, showing consecutive losses of water from secondary alcohol groups, as well as with tryptophan, characterized by indole ring formation and diagnostic ions at *m/z* 146.0601 (C_9H_8NO) and 188.0706 ($C_{11}H_{10}NO_2$). The molecular network and the observed spectral similarities reflected the theoretical grouping of different MR pathways, as previously hypothesized by Yaylayan[17]. Considering the similarities in the mass spectra, the Amadori compounds served as a key bridging point between amino acids and glucose, and they provided the basis for studying the spatial organization of the resulting degradation products.

To gain insight into the qualitative and quantitative relationships among the four model systems (two buffer systems and the emulsion systems after phase separation), we employed a supervised discriminant analysis based on fold change in logarithmic scale and post-hoc test. The results were summarized using a composite volcano plot of the emulsion system, comparing the two phases (PEG and Na_2SO_4) after separation at 5 h (Fig. 2, and Supplementary Data 3). In the green region, light blue points highlighted 33 discriminating compounds that were over-represented in PEG_5, as identified by a separate differential analysis between PEG_5 and

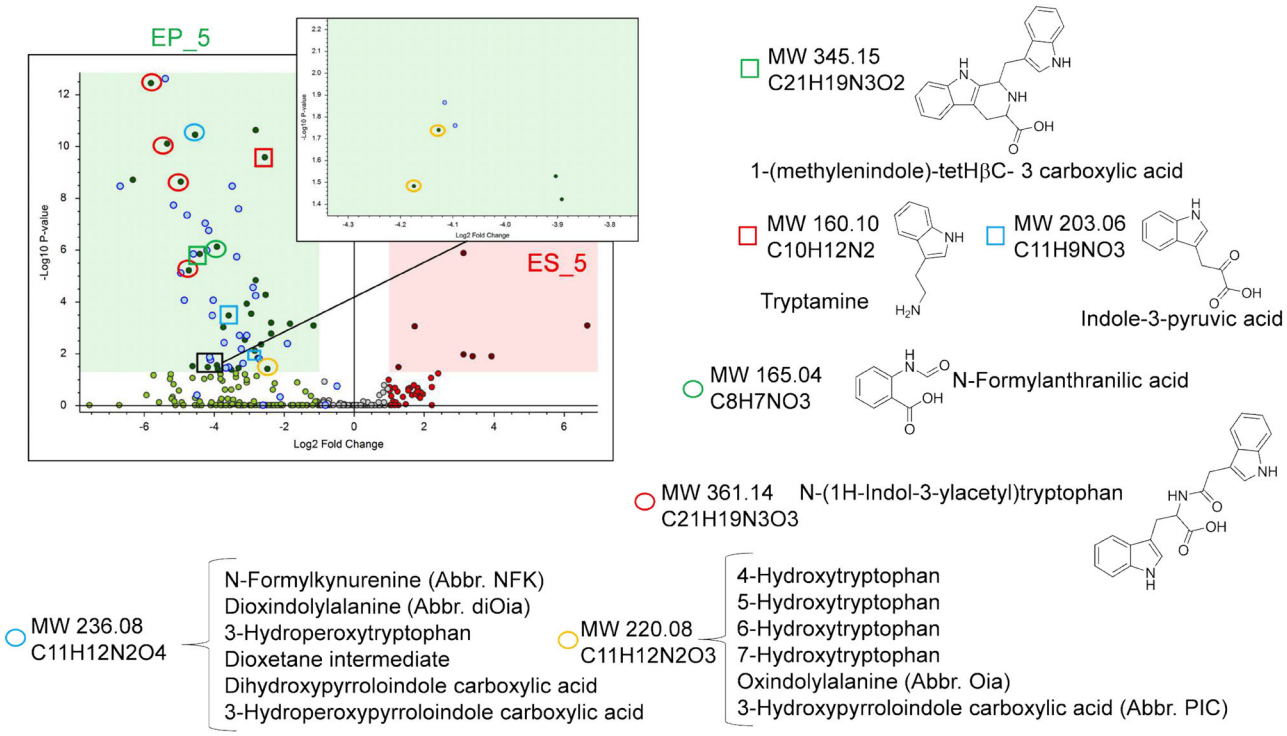

Fig. 2 | Composite volcano plot including the $\log_2$ fold change and $\log_{10}$ *p* value between EP_5 vs ES_5 for reactants segregation. Green areas report the compounds significantly over-represented in EP_5. Light blue-labeled points indicate compounds significantly over-represented in PEG_5 based on the discriminant analysis between PEG_5 and Na_2SO_4_5 (Supplementary Fig. S1 and Supplementary Data 1). Dark green points represent compounds significantly over-represented in EP_5, but not significantly over-represented in PEG_5 according to the same discriminant analysis. Red, blue, green, and yellow circles denote selected target compounds involved in reaction mechanisms, including direct tryptophan oxidation products, such as hydroperoxytryptophan and anthranilic acid. Blue, green, and red rectangles mark degradation and condensation products that involve tryptamine as a key reaction intermediate. EP (Emulsion PEG phase); ES (Emulsion Na_2SO_4 phase).

Na_2SO_4_5 (Supplementary Fig. 1). We subsequently performed manual curation of fragmentation spectra for target analytes present in EP_5 (Fig. 2 and inset with a magnified area). These analytes were highlighted using boxes of different shapes, corresponding to the reaction mechanisms illustrated in Figs. 3 and 4. Specifically, analytes were marked with yellow, green, blue, and red circles, as well as green, red, and blue rectangles, to represent distinct mechanistic categories.

Considering the evidence that Amadori compound rearrangement is likely to occur at the interface in the case of segregation mode[12], we propose that indole oxidation may predominate when reactants were segregated between the emulsion phases. Figure 3 illustrates the oxidation pathways initiated by tryptophan, along with trend lines showing the normalized area counts of the target analytes formed at 5 h. In Fig. 3A–D, we spotted the presence of four structural isomers peaking at *m/z* 361.1426 with molecular formula $C_{21}H_{19}N_3O_3$, different retention times, similar kinetic profiles and only one eluting at 4.8 min characterized by the predominance of typical fragmentation spectra of tryptophan ($C_{11}H_{10}NO_2$, *m/z* 188.0705; C_9H_8NO, *m/z* 146.0600; C_8H_8N, *m/z* 118.0650, as suggested by the molecular network in Fig. 1C and by the spectra in Supplementary Fig. 2A). In Supplementary Fig. 2B, fragment ion search (FiSH) scoring confirmed a structural match with *N*-(1H-indol-3-ylacetyl)tryptophan, suggesting the putative formation of an amide bond between 3-indoleacetic acid and tryptophan. This condensation is likely promoted under alkaline conditions and local dehydration, as reported by Marland et al.[18]. Next, we observed that oxidation products such as *N*-formylkynurenine and *N*-formylanthranilic acid were formed at significantly higher levels in the PEG phase, while they were detected only in lower amounts in Na_2SO_4 solution (Fig. 3E, F). The PEG phase, being a macromolecular environment, facilitated the condensation of hydrophobic compounds, enhancing the local concentration of tryptophan. In this phase, tryptophan was more likely to react with singlet oxygen, which was generated under thermal conditions, forming oxidative intermediates such as 3-hydroperoxytryptophan. These intermediates putatively promoted the formation of *N*-formylkynurenine, which underwent further transformation into *N*-formylanthranilic acid at temperature higher than 70 °C and in alkaline conditions[19]. The phase-specific environment thus played a relevant role in modulating the oxidation pathways and product formation. While for dioxindolylalanine, the distribution was in line with *N*-formylkynurenine, the two compounds 3-hydroperoxytryptophan and 3-hydroperoxypyrroloindole carboxylic acid exhibited a different behavior: their distribution in the emulsion upon phase separation was higher in PEG than salt phase, but both concentrations were strongly enhanced in Na_2SO_4 at 3 h.

Figure 4 summarizes the reaction pathways involved in the formation of condensation and polymerization products, with trend lines representing the normalized area counts of the target analytes at 5 h, 95 °C. Tryptamine, indole-3-pyruvic acid and 1-(3-methyleneindole)-tetHβC-carboxylic acid were formed at significantly higher levels in the PEG phase, while only in trace amounts were detected in Na_2SO_4 solution. The key intermediate tryptamine was formed via decarboxylation of tryptophan, while indole-3-pyruvic acid was produced through oxidative deamination[20]. Both intermediates underwent condensation, participating in the formation of β-carbolines derivatives and polymerization products. In the PEG phase, the macromolecular crowding effect could enhance the concentration of these reactants, thereby accelerating the condensation reactions and promoting the formation of β-carbolines. In the presence of reactive α-dicarbonyls, a specific class of β-carbolines can also be synthesized through intramolecular cyclization[21], leading to β-carbolines that are characterized by different logP depending on the type of α-dicarbonyls involved. In Supplementary Fig. 3, we reported the distribution of two compounds formed from the interaction between reactive carbonyls and tryptophan. Although 1-carboxyethyl-β-carboline shares

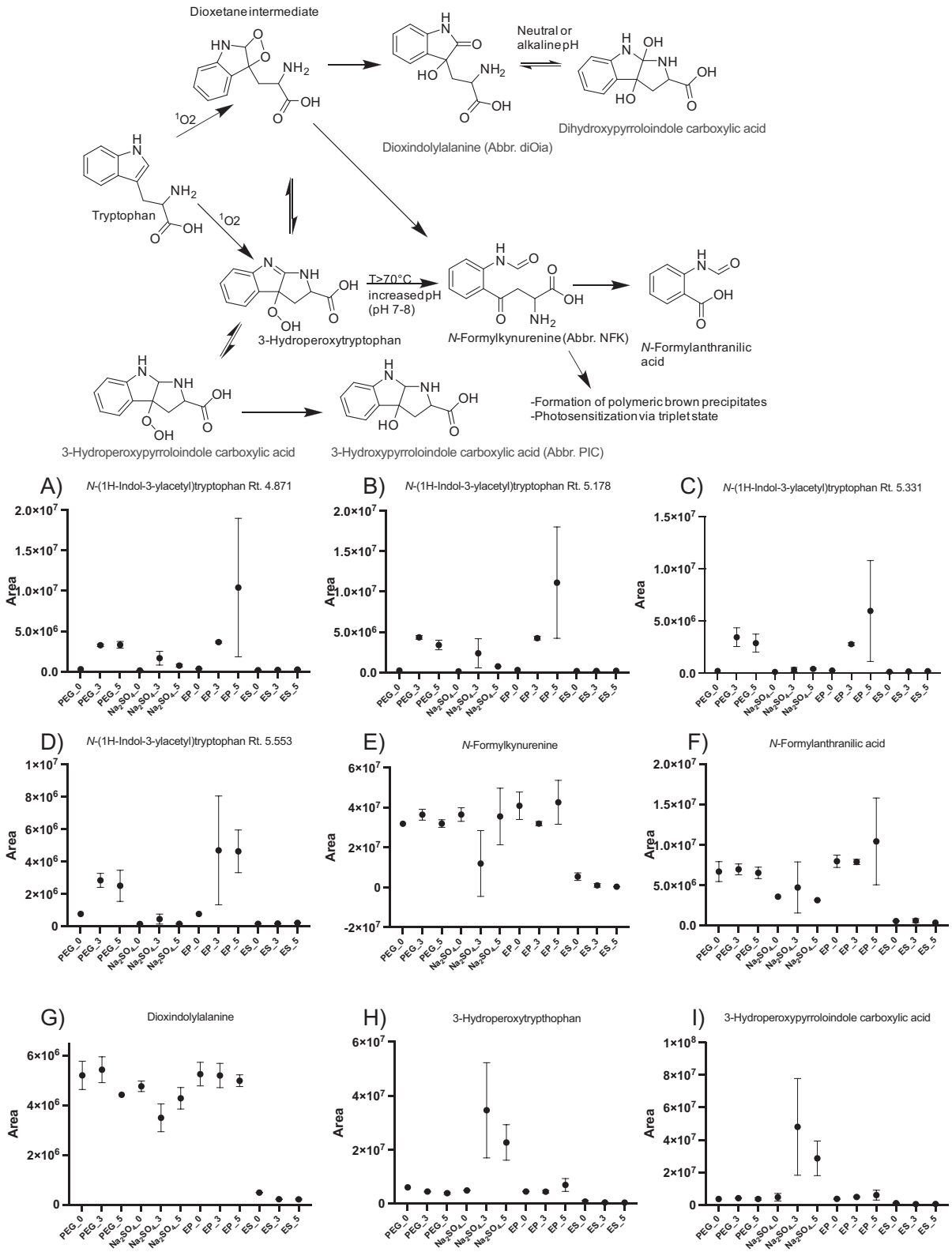

Fig. 3 | Tryptophan degradation products formed upon oxidation, including the generation of 3-hydroperoxytryptophan and a dioxetane intermediate according to Bellmaine et al[20]. These intermediates lead to the formation of *N*-formylkynurenine and *N*-formylanthranilic acid. Additionally, dioxyindolylalanine (diOia) was annotated as a precursor for the formation of a polymerization product. **A**–**I** Scatter plots of the normalized signal intensities of selected target analytes, obtained from full-scan experiments following annotation via tandem MS spectra. For structural isomers, the retention time was combined with the name or with the molecular formula. EP (Emulsion PEG phase); ES (Emulsion Na_2SO_4 phase); PEG (PEG solution); Na_2SO_4 (Na_2SO_4 solution); incubation time at 95 °C: 0, 3 and 5 h.

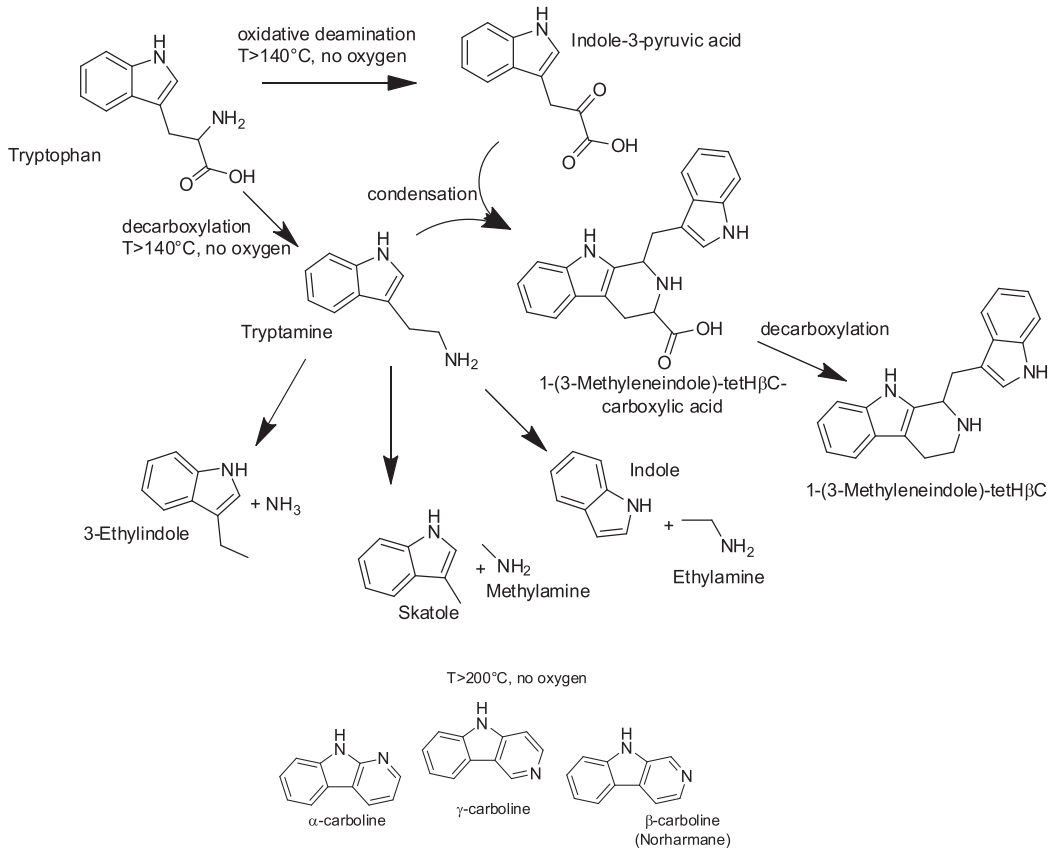

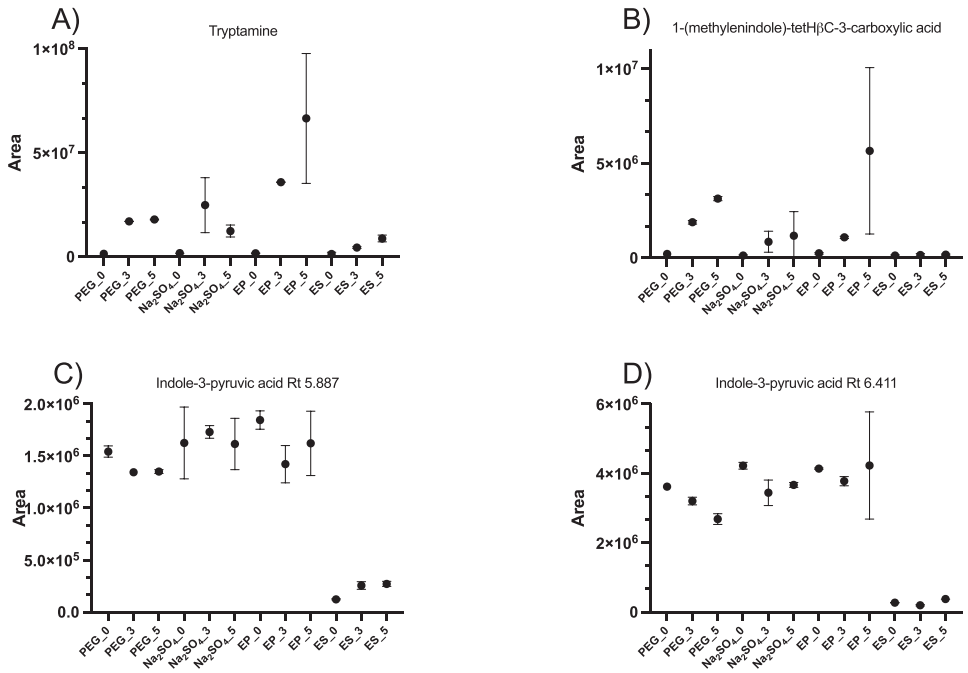

Fig. 4 | Tryptophan degradation products formed exclusively after heat exposure, with tryptamine, a decarboxylation product, as the key intermediate. Indole-3-pyruvic acid was included as a building block for further condensation reactions leading to the formation of carboline intermediates. The pathway also outlines the generation of fragmentation products such as ethylamine, which can react with reducing sugars to form amino-sugar compounds. Scatter plots in **A**–**D** present the normalized areas of target analytes identified in full-scan experiments following annotation and tandem MS spectrum identification. EP (Emulsion PEG phase); ES (Emulsion Na_2SO_4 phase); PEG (PEG solution); Na2SO4 (Na2SO4 solution); incubation time at 95 °C: 0, 3 and 5 h.

strong structural similarities with its propanoic acid derivative, their partitioning behavior differs significantly. Furthermore, tryptophan fragmentation products might have contributed to the generation of other compounds, including ethylamine and indole derivatives which can serve as indole building blocks for the formation of brown pigments and volatiles.

The approach used for PEG phase was extended to the study of Na_2SO_4 phase: Fig. 5 and Supplementary Data 3 show the composite volcano plot comparing ES and EP at 5 h. The 42 light blue compounds pinpoint those over-represented in the Na_2SO_4 phase compared to the PEG buffer phase (Supplementary Fig. 1). As expected, none of the compounds that were over-represented in the Na_2SO_4 solution at 5 h maintained the same pattern in the emulsion system. All were distributed below the green and red regions, indicating very low $-\log_{10} p$-values and, thus, a weak discriminative power. This strategy enabled the identification of compounds significantly enriched in the Na_2SO_4 phase after phase separation and facilitated the investigation of how compounds migrate from the PEG phase to the Na_2SO_4 phase. Such compounds were highlighted using red, purple, blue, and yellow triangles. The semi-quantitative trends shown in Fig. 5 were consistent across datasets: a pronounced and statistically significant increase in the Na_2SO_4 phase after phase separation, with negligible signals detected in the other model systems. One exception was represented by the compound with formula $C_6H_{11}NO_4$, annotated and putatively identified as 6-amino-4,5-dihydroxyhexan-2,3-dione, a dehydration product of glycosylamine, which was formed at comparable levels in both Na_2SO_4 solution and Na_2SO_4 phase (Na_2SO_4 and ES). Here, most of the compounds originated from the glucose moiety, with some amino-sugar derivatives putatively formed at the interface, as in the case of the compound with molecular formula $C_{12}H_{23}NO_{10}$, putatively assigned as a hexose derivative of glycosylamine[22]. None of the indole derivatives were detected at significant levels among the over-represented molecules.

Asparagine and glucose reactivity in reactants co-encapsulation

Figure 6 provides an overview of the 2D distribution of samples and compounds annotated when reactants were co-encapsulated (asparagine and glucose model system). This analysis compares data at time 0 and at 5 h of thermal treatment at 95 °C. The PCA in Fig. 6A explained a total variance of 53.0%, with a more complex sample distribution than observed in reactants segregation. Indeed, the higher contribution of PC1 (32.1%) pointed to an effect of composition rather than an effect due to reaction time. At time 0, all the samples were characterized by negative values of the PC2. At 5 h, the samples shifted along the second principal component (accounting for 20.9% of the variance), all exhibiting positive PC2 values. This distribution highlighted key differences already present at time 0, suggesting that the preparation of the model system (including pre-incubation, mixing, and dissolution) induced the formation of early-stage reaction products. This interpretation is supported by the loadings plot in Fig. 6B, where grey data points of annotated compounds clustered around black points along both axes, indicating a greater contribution from Na_2SO_4-containing systems (Na_2SO_4 solution and ES at time 0 and at 5 h).

Figure 6C depicts the interconnection between the fragmentation spectra of asparagine, glucose, and their respective reaction products. As for tryptophan segregation model system, the Amadori compound of asparagine (*N*-(1-deoxy-L-fructos-1-yl)-D-asparagine, Fru-Asn) is between two molecular clusters representing amino acid degradation products and glucose degradation products, underlined in red and blue boxes, respectively. This distribution confirmed what was observed for tryptophan: the Amadori rearrangement remained the main driver for the Maillard reaction in both reactant segregation and co-encapsulation in the presence of free amino group and reducing sugars. Besides the linkages between the two clusters, a closer relationship was observed between the Amadori compound of asparagine and several degradation products, most of which are small organic acids. Here, we hypothesize that the carbohydrate moiety of the Amadori compound contributes more efficiently to the generation of fragmentation products than tryptophan (or that, in the case of tryptophan, the reactivity of the indole rings predominated), likely due to the preferred intramolecular rearrangement of indole rings with dicarbonyl compounds. As in reactant segregation, the co-encapsulation molecular network was constructed across the four model systems without using time as a discriminating variable according to the similarities in the fragmentation spectra.

To provide information on the spatial organization of reactants co-encapsulation, a composite volcano plot was developed in Fig. 7 and Supplementary Data 4 ($\log_2$ fold change > 1 and $\log_{10}$ *p*-value > 1.3). As a preliminary step, 38 compounds that were over-represented in PEG compared to Na_2SO_4 solution at 5 h (Supplementary Fig. 4) were outlined in light blue in Fig. 7. This strategy favored an initial screening of compounds significantly enriched or accumulated in the PEG phase after phase separation. Among the 16 compounds over-represented in EP (green region in Fig. 7), four annotated compounds were further highlighted using red, blue, green, and yellow circles. Three compounds exhibited similar fragmentation spectra characterized by an intense signal at *m/z* 96.96. This conserved and prominent signal was indicative of a sulfate ion fragment. We hypothesize that reactions involving sulfate moieties occurred in the Na_2SO_4 phase, with subsequent cyclization products migrating into the PEG phase. Indeed, 1H-pyrrole-2-carboxamide served as a key example of a pyrrole derivative that moves between the two regions, accumulating in the PEG phase or a controlled reaction rate in the Na_2SO_4 phase.

In parallel, Fig. 8 presents the same composite volcano plot shown in Fig. 7, with light blue-labeled points derived from the discriminant analysis between Na_2SO_4 and PEG solutions at 5 h and shown in the red region. According to this layout, we identified the compounds that accumulated in the Na_2SO_4 phase after phase separation, excluding the 29 compounds over-represented in Na_2SO_4 based on the PEG vs. Na_2SO_4 discriminant analysis (Supplementary Fig. 4). Figure 8A, B illustrate two examples of pyridine derivatives that accumulated significantly in the Na_2SO_4 phase, while remaining at very low concentrations in both PEG and EP. Figure 8C summarizes the time-dependent trend of 3-deoxyglucosone that although hydrophilic, its normalized area counts were comparable between the ES and EP. Notably, an increasing trend over time was observed only in the Na_2SO_4 phase after phase separation, suggesting its distribution among both phases. These results pinpointed that compounds formed in the Na_2SO_4 phase may continue to migrate between phases, influenced by reaction conditions such as pH, time and temperature.

In addition to asparagine degradation products, we identified other markers of asparagine oxidation: aspartyl-asparagine and asparaginyl-aspartic acid, two dipeptide isomers that eluted at different retention times but displayed identical fragmentation spectra (Supplementary Fig. 5A). In Supplementary Fig. 5B, we reported the MS/MS spectrum with FiSH scoring for the putative chemical compound including the formation of a peptide bond between aspartic acid and asparagine. Both isomers may originate from the initial oxidation of asparagine to aspartic acid, followed by further peptide bond formation and oxidation. Despite amine acylation in water is a common reaction in the presence of dedicated enzymes, this process occurs rarely in the absence of catalysts; this is because the high concentration of water shifts the equilibrium toward hydrolysis. In the present work, we observed the formation of the peptide bond probably as result of the alteration of the local water concentration due the different reagent partitioning or the occurrence of a base-catalyzed process at the hydrophobic interfacial compartment that promoted the formation of the necessary tetrahedral reaction intermediate[23]. Finally, as reported in the Fig. 8H, the increase in the response of the glycosylamine derivative paralleled the trend observed for the tryptophan model system.

Reactants co-encapsulation and segregation introduce the space as a control parameter for chemical reactions

All-aqueous emulsions influence the spatial distribution of reactants based on the intrinsic chemical properties of the precursors, thereby affecting overall chemical reactivity and contributing to system stabilization[24]. The contrast between co-encapsulation and segregation, as specific modes of compartmentalized reactions, allowed the spatial separation of glucose, asparagine, and tryptophan within the two immiscible aqueous phases of

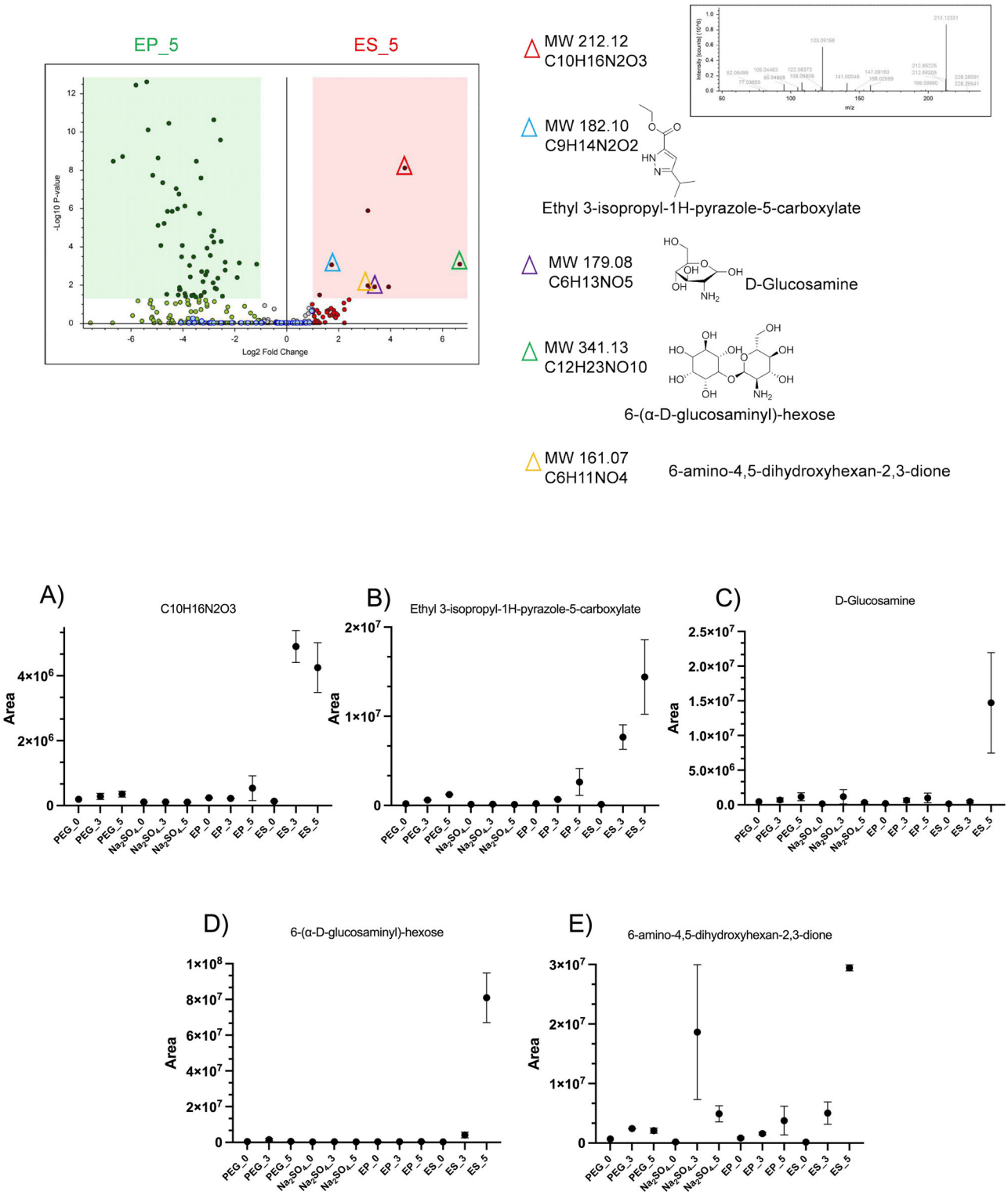

Fig. 5 | Compounds identification in reactants segregation through discriminant analysis. Composite volcano plot including the log2 fold change and log10 *p* value between EP_5 vs ES_5 for reactants segregation, following the arrangement reported in Fig. 2, in Supplementary Fig. S1 and Supplementary Data 3. Red areas report the compounds significantly over-represented in ES_5. Light blue-labeled points indicate compounds significantly over-represented in Na_2SO_4_5 based on the discriminant analysis between PEG_5 and Na_2SO_4_5 (Supplementary Fig. S1). Dark red points represent compounds significantly over-represented in ES_5 but not significantly enriched in Na_2SO_4_5 according to the same discriminant analysis. Red, blue, purple, green, and yellow triangles mark target compounds involved in proposed reaction mechanisms, including direct glucose oxidation products and other intermediate degradation products. Scatter plots in **A**–**E** show the normalized areas of target analytes identified in full-scan experiments following annotation and tandem MS spectral identification. EP (Emulsion PEG phase); ES (Emulsion Na_2SO_4 phase); PEG (PEG solution); Na_2SO_4 (Na_2SO_4 solution); incubation time at 95 °C: 0, 3 and 5 h.

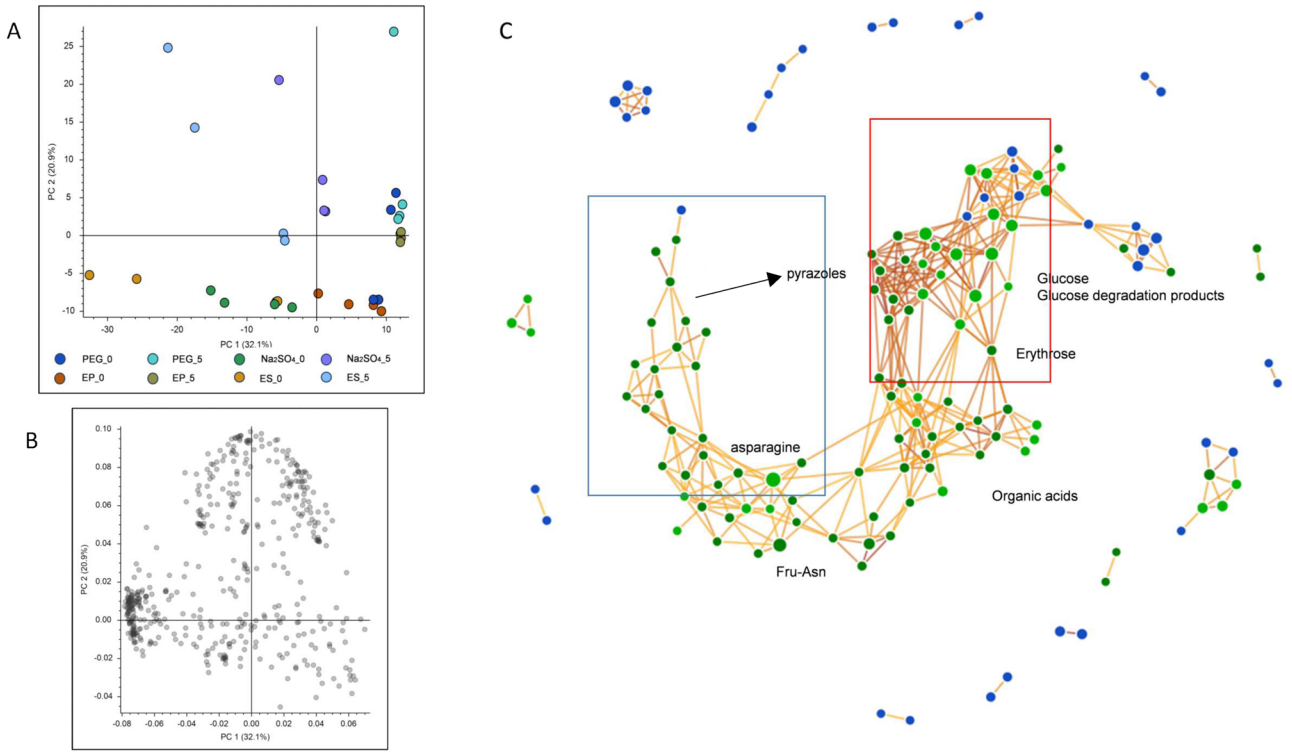

Fig. 6 | 2D sample distribution, compound loadings plot, and molecular networking upon filtering procedure of ddMS² experiments for reactants co-encapsulation. A The PCA of the four model systems at time 0 and after 5 h at 95 °C. Colors indicate different time points (0 vs. 5 h) and systems: EP (Emulsion PEG phase), ES (Emulsion Na_2SO_4 phase), PEG (PEG solution), and Na_2SO_4 (Na_2SO_4 solution). **B** The compound loadings plot, with dark grey indicating compound accumulation after 5 h at 95 °C. **C** The chemical space, including glucose, asparagine, and their putative degradation products, linked via the Amadori compound of asparagine (Fru-Asn). Identified molecules are shown in green scale according to their level of identification, whereas unknowns are reported in blue. Yellow lines connect compounds with similar fragmentation patterns in ddMS². The network was built across all four systems without using time as a grouping variable, to reveal relationships among precursors, intermediates, and end-products based on the similarities between high-resolution tandem MS spectra.

the all-aqueous emulsions studied here through HILIC-HRMS. Metabolomics elucidated the complex interplay among time, temperature, reactant localization, and the final distribution of end-products within the emulsion system. Comparing amino acids and sugars separation across the phases with their coexistence within a single phase controlled the execution of the sequential transformations characteristic of the Maillard cascade, including the formation of the Amadori compounds and related oxidation processes[12]. We demonstrated that melanoidin building blocks can migrate from one phase to another, representing an extreme case of on-droplet formation. The selective partitioning of the two amino acids into specific phases or at the interface increased their local concentrations at the reaction sites, thereby enhancing reaction rates in accordance with the principles of mass action.

As previously reported by our group, the partition coefficients of amino acids regulate the localization of side chains in all-aqueous emulsions and influence the formation of reaction end-products[12]. We observed that the localization of precursors, whether coexisting within droplets as in the case of asparagine and glucose or spatially separated at the interface as with tryptophan and glucose, can lead to the formation of distinct reaction products because of the intrinsic chemical nature of the precursors (reactants location) and the subsequent distribution of the resulting products within all-aqueous emulsions. Specifically, tryptophan and glucose first reacted at the interface to form the corresponding Amadori compound, then this intermediate migrated into the PEG phase. In addition to participating in the Maillard reaction, tryptophan underwent oxidation. In this context, it has been reported that tryptophan can form 3-hydroperoxytryptophan, 3-hydroperoxypyrroloindole carboxylic acid and a dioxetane intermediate through oxidation pathways, both of which are proposed precursors to *N*-formylanthranilic acid[20]. Furthermore, tryptophan may undergo oxidative deamination to yield indole-3-pyruvic acid and decarboxylation to produce tryptamine, as reported here for the reactant segregation mode. The condensation of these two compounds can lead to the formation of 1-(methylenindole)-tetrahydro-β-carboline-3-carboxylic acid, a β-carboline derivative. Notably, these transformation pathways are typically activated under high-temperature or in anaerobic conditions (up to 140 °C), as described by Bellmaine et al.[20]. Maillard reaction intermediates and advanced products, such as carbonyl compounds, pyridines, quinones, and pyrroles, often carry reactive functional groups with oxidative properties that can generate free radicals[25], contributing to the chemical complexity of the system with propagation reactions, consistent with previous observations in oil-in-water emulsions[26]. Indeed, the co-localization of these MR products and tryptophan within the PEG phase likely promoted the oxidative transformation of tryptophan, either by reaction with α-dicarbonyls or through the generation of reactive oxygen species, which can also be formed from the degradation of PEG. These processes may have led to modifications in the overall supramolecular arrangement of the all-aqueous system. The results suggest that reactant segregation not only directs initial Maillard reaction steps but also modulates the fate of amino acid-derived intermediates through selective partitioning and the resulting localized reactivity.

The reaction between glucose and asparagine in all-aqueous emulsion is influenced when reactants are segregated between the emulsion phases. The co-encapsulation of the reaction precursors within the Na_2SO_4 phase enabled the Maillard reaction to proceed in a compartmentalized manner. Specifically, glycosylamines were significantly partitioned into the Na_2SO_4 phase and subsequently underwent the Amadori rearrangement. The resulting Amadori products then degraded to form reactive α-dicarbonyl compounds, such as 3-deoxyglucosone[27]. We hypothesize that under these conditions, glucose may have undergone rearrangement, subsequent nucleophilic addition by amines, potentially leading to the formation of a

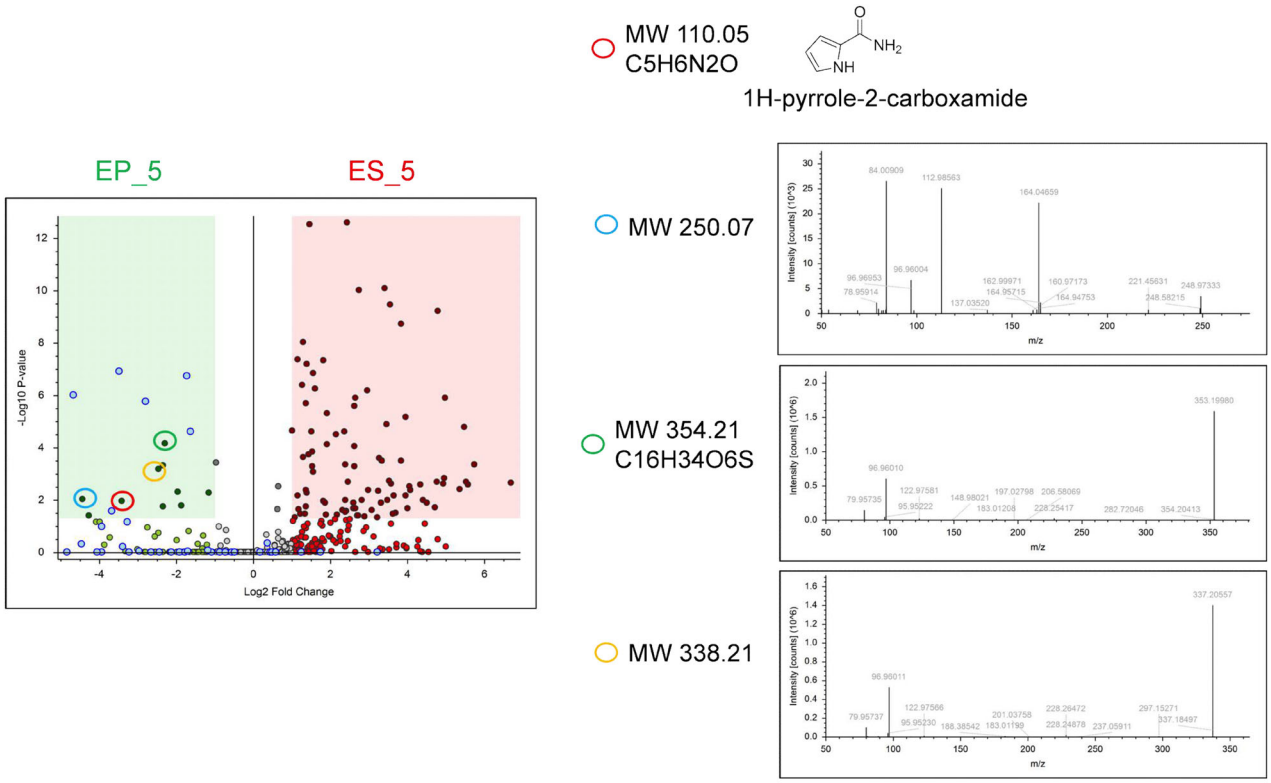

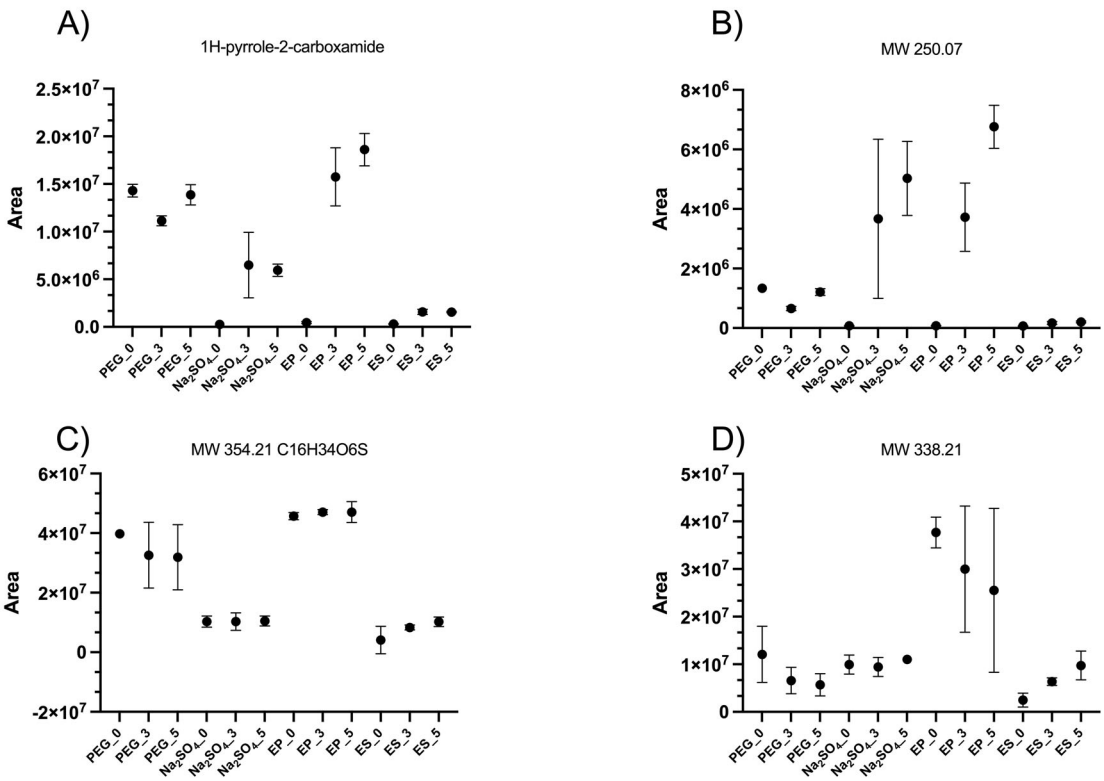

Fig. 7 | Composite volcano plot including the log_2 fold change and log_{10} *p* value between EP_5 vs ES_5 for reactants co-encapsulation. Green area reports the compounds significantly over-represented in EP_5 and Supplementary Data 4. Light blue-labeled points indicate compounds significantly over-represented in PEG_5 based on the discriminant analysis between PEG_5 and Na_2SO_4_5 (Supplementary Fig. S4). Dark green points represent compounds significantly over-represented in EP_5, but not significantly over-represented in PEG_5 according to the same discriminant analysis. Red, blue, green and yellow circles are representative of the target compounds part of the reaction mechanisms including direct asparagine cyclization and oxidation products as pyrrole derivatives. Scatter plots in **A**–**D** include the normalized areas of target analytes screened in full scan experiments upon annotation of tandem MS spectra with fragment pointing at *m/z* 96.96. EP (Emulsion PEG phase); ES (Emulsion Na_2SO_4 phase); PEG (PEG solution); Na_2SO_4 (Na_2SO_4 solution); incubation time at 95 °C: 0, 3 and 5 h.

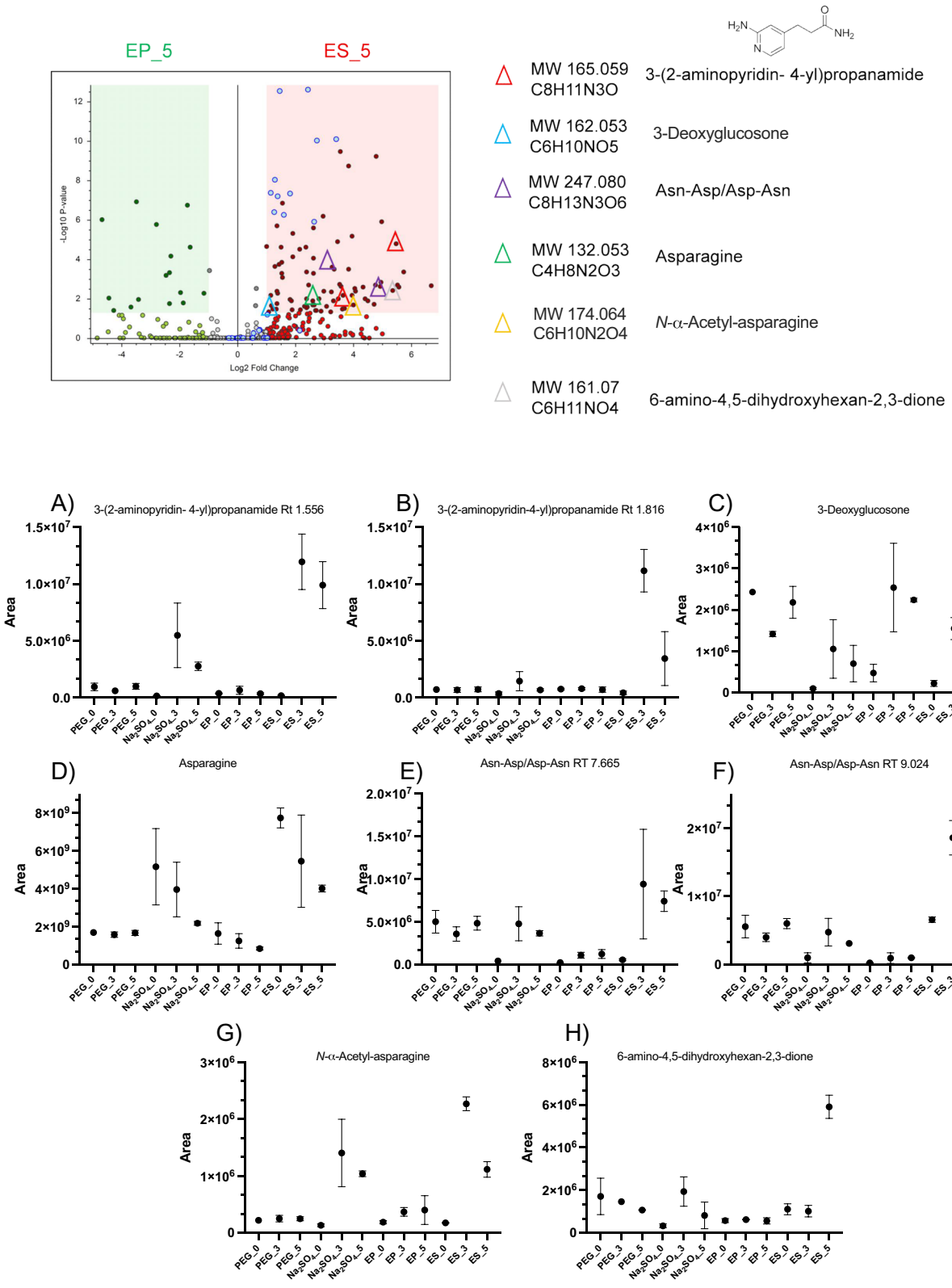

Fig. 8 | Composite volcano plot including the $\log_2$ fold change and $\log_{10}$ *p* value between EP_5 vs ES_5 for reactants co-encapsulation, following the layout used in Fig. 7. Red areas report the compounds significantly over-represented in ES_5 and Supplementary Data 4. Light blue-labeled points indicate compounds significantly over-represented in Na_2SO_4_5 based on the discriminant analysis between PEG_5 and Na_2SO_4_5 (Supplementary Fig. S4). Dark red points represent compounds significantly over-represented in ES_5 but not significantly enriched in Na_2SO_4_5 according to the same discriminant analysis. Red, blue, purple, green, yellow, and grey triangles mark target compounds involved in proposed reaction mechanisms, including direct glucose oxidation products and other intermediate degradation products. Scatter plots in **A**–**H** show the normalized areas of target analytes identified in full-scan experiments following annotation and tandem MS spectral identification. EP (Emulsion PEG phase); ES (Emulsion Na_2SO_4 phase); PEG (PEG solution); Na_2SO_4 (Na_2SO_4 solution); incubation time at 95 °C: 0, 3 and 5 h.

stable six-membered ring compound, putatively identified as 6-amino-4,5-dihydroxyhexan-2,3-dione.

Asparagine is known to undergo non-enzymatic deamidation under physiological or elevated temperature conditions. This process involves the formation of a cyclic imide intermediate, which is unstable and subsequently hydrolyzed to yield a mixture of L-aspartic acid (Asp) and L-isoaspartic acid. Here, we propose that Asp and Asn may undergo a condensation reaction to form dipeptides such as Asn–Asp or Asp–Asn. However, peptide bond formation from free amino acids in aqueous solution is thermodynamically unfavorable due to the high-water activity and the lack of catalyzing agents[28]. Nevertheless, under our experimental conditions, factors such as reduced water activity, selective partitioning, alkaline pH, and local microenvironments with limited hydration may have helped in shifting the equilibrium toward peptide bond formation. It is therefore possible that the high salt concentration in the Na_2SO_4 phase created a dehydrating environment that facilitated this reaction[29]. Taken together, the co-encapsulation of glucose and asparagine within the Na_2SO_4 phase created a microenvironment with reduced water activity and elevated local reactant concentrations, thereby facilitating condensation reactions such as the Amadori rearrangement and possibly peptide bond formation in the absence of conventional catalyzing agents. Of note, a similar pathway was also observed in the case of segregation mode with the formation of *N*-(1H-indol-3-ylacetyl)tryptophan, as a reaction product between 3-indoleacetic acid and tryptophan. In both segregation and co-encapsulation cases, the use of labeled precursors, ion mobility mass spectrometry, advanced techniques as NMR, multiresponse modeling at different time/temperature profiles and testing the system in absence of glucose can provide further structural confirmation to those observed here by tandem mass spectrometry.

Conclusions

Overall, our findings highlight how all-aqueous emulsions can drive distinct chemical trajectories for amino acids and sugars, with broad implications across various reaction types. The reaction intermediates and products generated within these systems can, in turn, influence other processes, as shown here for oxidation and peptide bond formation. Indeed, the selective partitioning of reactants and intermediates into PEG or Na_2SO_4 phases directs canonical glycation reactions and fosters oxidation and condensation transformations that are otherwise suppressed in homogeneous aqueous systems. These findings provide new insights into how microenvironmental factors, such as water activity and reactant concentration, can be harnessed to modulate reaction pathways and product profiles in complex food matrices. Finally, we demonstrated that spatial compartmentalization, beyond traditional parameters like time, pH, viscosity, and temperature, is a critical factor in governing all the above-mentioned reactions.

Material and methods

Chemicals and reagents

Acetonitrile and water were purchased from Merck-Sigma-Aldrich (Darmstadt, Germany); D-glucose, D-galactose, L-tryptophan, tryptamine, L-asparagine, N-α-acetyl-asparagine, polyethylene glycol (PEG) 8 kDa, sodium sulfate (Na_2SO_4), phosphate buffer powder, ammonium formate and formic acid were purchased from Merck-Sigma-Aldrich. *N*-(1-deoxy-D-fructos-1-yl)-L-tryptophan (Fru-Trp) and *N*-(1-deoxy-D-fructos-1-yl)-L-asparagine (Fru-Asn) were purchased from Toronto Research Chemicals (Toronto, Canada). All chemicals used in this study were of analytical grade, except for liquid chromatographic solvents, water and acetonitrile that were of mass spectrometry grade.

Preparation of all-aqueous droplet reactors

All-aqueous droplet reactors were prepared according to the method described in our previous paper[12]. Na_2SO_4 and PEG were used as phase-forming components that defined the two aqueous phases governing the spatial organization and reactivity of the precursors. Na_2SO_4 acted as the component that forms the inner droplet phase, providing a highly hydrated yet ion-rich microenvironment where hydrophilic reactants such as glucose and asparagine can become compartmentalized. Conversely, PEG constituted the continuous outer phase and induced macromolecular crowding. The PEG-rich environment concentrated hydrophobic reactants, facilitating condensation and polymerization processes that yielded different products. The concentrations of Na_2SO_4 and PEG were 171.6 g L^{-1} and 551.0 g L^{-1}, respectively.

To prepare the all-aqueous droplet reactors, aqueous stock solutions of Na_2SO_4 (15 wt%) and PEG (50 wt%) were prepared by the addition of either Na_2SO_4 or PEG to phosphate buffer stock solution (0.1 M, pH 7.4). All-aqueous droplet reactors (Na_2SO_4/PEG) were prepared by mixing the Na_2SO_4 and PEG stock solutions at a volume ratio of 1:4, with stirring at 1000 rpm for 1 h. Subsequently, the droplet reactors were supplemented with the Maillard reactants (glucose and either asparagine or tryptophan), achieving a final concentration of 40 mM. The mixtures were stirred overnight at 25 °C for complete dissolution of the reactants. After phase separation, PEG phase (EP) and Na_2SO_4 phase (ES) were collected from samples. For comparison purposes, in addition to the droplet reactor samples (two-phase systems), single-phase solutions were also prepared. These included mixtures of phosphate buffer solution and Na_2SO_4 or PEG stock solutions (referred to as "Na_2SO_4" and "PEG", respectively). All these solutions were supplemented with the same reactants.

Running the MR in droplet reactors and single-phase solutions

The reactants-supplemented emulsions (and single-phase solutions, 5 mL) were transferred into gas chromatography vials (20 mL) and securely sealed. Subsequently, these vials were heated at 95 °C for 0 h, 3 h, and 5 h while being stirred at 1000 rpm. Next, the samples were rapidly cooled within an ice bath, then kept at room temperature (25 °C) for 4 h. The top and bottom phases were then diafiltrated (molecular weight cut-off 3000 Da) at 14,000 × *g*, repeated five times, with each cycle lasting 30 min. Both the retentate and permeate fractions were collected and subsequently freeze-dried (Alpha 2-4 LD plus, Martin Christ, Osterode am Harz, Germany) for further analysis. For comparison purposes, the single-phase samples supplemented with the reactants were also stored at 25 °C for 4 h and diafiltrated. These single-phase systems served as control samples to decouple the effects of phase separation from those of the chemical composition. In particular, the single-phase systems allowed us to verify whether the changes in reaction pathways and product distributions were due to the compartmentalization and reactant localization in the all-aqueous emulsions rather than the intrinsic chemical properties of PEG or Na_2SO_4.

Liquid chromatography high-resolution mass spectrometry

The formation of reaction products of asparagine and tryptophan was screened in untargeted mode in emulsion systems after phase separation by using PEG solution and Na_2SO_4 solution as controls. Freeze-dried permeates were redissolved in water, and both the upper and lower phases were diluted in 50% aqueous acetonitrile, then centrifuged (18,000 × *g*, 4 °C, 10 min). LC-MS/MS data were acquired using an Exploris 120 quadrupole Orbitrap high-resolution mass spectrometer interfaced to a Vanquish Core liquid chromatographic system (Thermo Fisher Scientific, Bremen, Germany). Compounds were separated at 40 °C through a zwitterionic sulfobetaine column (Atlantis Premier BEH, Z-HILIC, 100 ×2.1, 1.7 µm, Waters) with the following gradient of solvent B (minutes/%B): (0/5), (1.5/5), (10/50), (13/50). Mobile phases consisted of 0.1% formic acid in acetonitrile (v/v, solvent A) and 0.1% formic acid in water (v/v, solvent B); the flow rate was 0.3 mL min^{-1}. Samples were acquired in profile data-dependent scanning ($ddMS^2$) mode by using polarity switching. For positive ion (and negative ion) mode, H-ESI interface parameters were as follows: static spray voltage 3.3 kV (−2.9 kV), while ion transfer tube and vaporizer temperature were both at 280 °C; sheath gas flow and auxiliary gas flow were 38 and 8 arbitrary units, respectively, for both positive and negative ion mode. Along with full scan acquisition in the *m/z* range 60–900 (resolution 60,000 at *m/z* 200 FWHM), $ddMS^2$ were performed on the top 4 scans by using an intensity threshold of 60,000 (area counts), a customized dynamic exclusion window of 3.5 s and a mass

tolerance of 5 ppm. A targeted mass exclusion list was incorporated within the LC-MS/MS method upon the analysis of two separated full scan acquisition runs of blank samples and the removal of the top 600 most intense background signals, for both positive and negative ion mode. Finally, $ddMS^2$ scan properties included an isolation window of *m/z* 1.5, a normalized higher energy collisional dissociation of 20%, 40% and 80% and the Orbitrap resolution fixed at 30,000. Data were acquired in profile mode by using a standardized AGC (all gain control) target and EASY-IC® (fluoranthene as internal calibrant) at the beginning of each run. Identification of precursors, putative intermediates and end-products along with area counts normalization and peak alignment were achieved by injecting pooled quality control samples at regular intervals of 6 runs and by analyzing reference mixes through differential scanning ranges (*m/z* 60–200, *m/z* 190–400, *m/z* 390–600 and *m/z* 590–900) in both positive and negative mode by using the same chromatographic layout as described above.

Untargeted metabolomics

An untargeted metabolomic workflow based on reaction product identification was used to find and characterize differences between the buffer control samples and fully aqueous emulsions in the presence of asparagine and glucose or tryptophan and glucose by importing raw files in Compound Discoverer software (v. 3.3 Thermo Fisher Scientific, San José, CA). The procedure involved the retention time alignment and detection of expected and unknown compounds for sample grouping. Upon definition of the elemental composition, exact masses, chemical formulas and fragmentation spectra, compounds were matched with analytical standards as glucose, tryptophan, asparagine and their respective Amadori compounds. The procedure encompassed the generation of five separated libraries including end-products with a similar fragmentation pattern. This strategy generated two distinct molecular networks that were combined with analytical information reported in publicly available databases, as mzCloud (www.mzcloud.org) and ChemSpider (www.chemspider.com). A supplementary search was performed in Reaxys® (Elsevier, Amsterdam, the Netherlands) by using as reactants the two amino acids and glucose, with temperature higher than 50 °C, to generate an internal mass list of putative chemical structures arising from the model systems. After correction for quality control samples, post-processing nodes performed descriptive statistics and differential analysis working on two technical replicates arising from two replicates representative of four observations for each time point/condition. For volcano plots and ratios among sample groups, *p*-values were adjusted by Benjamini–Hochberg algorithm. Tandem MS spectra, PCA, histograms, scatter plot, loadings plots, molecular network[13], statistical test, and log fold changes were obtained in Compound Discoverer. Reaction pathways and chemical structures were built in ChemDraw (Revvity Signals Software, Waltham, MA). Dataset with all the numerical data related to Figs. 1 to 8 is reported in Supplementary Data 5.

Data availability

All the data generated or analyzed during this study are included in this published article (and in its supplementary information files). Data are available upon request under the responsibility of the corresponding author.

Received: 6 August 2025; Accepted: 12 February 2026;
Published online: 21 March 2026

References

1. Ruiz-Lopez, M. F., Francisco, J. S., Martins-Costa, M. T. C. & Anglada, J. M. Molecular reactions at aqueous interfaces. *Nat. Rev. Chem.* **4**, 459–475 (2020).
2. Madadlou, A., Saggiomo, V., Schroen, K. & &Fogliano, V. All-aqueous emulsions as miniaturized chemical reactors in the food and bioprocess technology. *Curr. Opin. Food Sci.* **33**, 165–172 (2020).
3. Shakoor, A., Zhang, C., Xie, J. & &Yang, X. Maillard reaction chemistry in formation of critical intermediates and flavour compounds and their antioxidant properties. *Food Chem.* **393**, 133416 (2022).
4. Gao, Y., Miao, J. & &Lai, K. Study on Maillard reaction mechanism by quantum chemistry calculation. *J. Mol. Model.* **29**, 81 (2023).
5. Mottram, D. S. The Maillard reaction: source of flavour in thermally processed foods. in *Flavours and Fragrances: Chemistry, Bioprocessing and Sustainability* (ed Berger, R. G.) (Springer Berlin Heidelberg, 2007).
6. Murata, M. Browning and pigmentation in food through the Maillard reaction. *Glycoconj. J.* **38**, 283–292 (2021).
7. Bork, L. V., Haase, P. T., Rohn, S. & &Kanzler, C. Structural characterization of polar melanoidins deriving from Maillard reaction intermediates - A model approach. *Food Chem.* **395**, 133592 (2022).
8. van Boekel, M. A. Kinetic aspects of the Maillard reaction: a critical review. *Nahrung* **45**, 150–159 (2001).
9. Hellwig, M. & &Henle, T. Baking, ageing, diabetes: a short history of the Maillard reaction. *Angew. Chem. Int. Ed.* **53**, 10316–10329 (2014).
10. Weidner, L., Cannas, J. V., Rychlik, M. & &Schmitt-Kopplin, P. Molecular characterization of cooking processes: a metabolomics decoding of vaporous emissions for food markers and thermal reaction indicators. *J. Agric. Food Chem.* **71**, 17442–17454 (2023).
11. Zhou, Z. et al. Unraveling the thermal oxidation products and peroxidation mechanisms of different chemical structures of lipids: an example of molecules containing oleic acid. *J. Agric. Food Chem.* **70**, 16410–16423 (2022).
12. Chen, K. et al. Compartmentalization vs. segregation of reactants: Accomplishment of the Maillard reaction at the water-water interface. *Food Chem.* **465**, 142089 (2025).
13. Schmid, R. et al. Ion identity molecular networking for mass spectrometry-based metabolomics in the GNPS environment. *Nat. Commun.* **12**, 3832 (2021).
14. Yan, Y., Hemmler, D. & Schmitt-Kopplin, P. Discovery of glycation products: Unraveling the unknown glycation space using a mass spectral library from in vitro model systems. *Anal. Chem.* **96**, 3569–3577 (2024).
15. Kaufmann, A. High-resolution mass spectrometry for bioanalytical applications: Is this the new gold standard? *J. Mass Spectrom.* **55**, e4533 (2020).
16. Sumner, L. W. et al. Proposed minimum reporting standards for chemical analysis: chemical analysis working group (CAWG) metabolomics standards initiative (MSI). *Metabolomics* **3**, 211–221 (2007).
17. Yaylayan, V. A. Classification of the Maillard reaction: a conceptual approach. *Trends Food Sci. Technol.* **8**, 13–18 (1997).
18. Marland, E. et al. Robust synthesis of prebiotic precursors in drying reactions of amino acids and keto acids. *ChemSystemsChem* **8**, e00018 (2025).
19. Ronsein, G. E., Oliveira, M. C., Miyamoto, S., Medeiros, M. H. & Di Mascio, P. Tryptophan oxidation by singlet molecular oxygen [O2(1Deltag)]: mechanistic studies using 18O-labeled hydroperoxides, mass spectrometry, and light emission measurements. *Chem. Res. Toxicol.* **21**, 1271–1283 (2008).
20. Bellmaine, S., Schnellbaecher, A. & Zimmer, A. Reactivity and degradation products of tryptophan in solution and proteins. *Free Radic. Biol. Med.* **160**, 696–718 (2020).
21. Herraiz, T., Peña, A., Mateo, H., Herraiz, M. & Salgado, A. Formation, characterization, and occurrence of β-carboline alkaloids derived from α-dicarbonyl compounds and L-tryptophan. *J. Agric. Food Chem.* **70**, 9143–9153 (2022).
22. Fischer, N. H. & Pedersen, C. M. Chemical glycosylations in water and aqueous media. *Chem. Rev.* **125** 12069–12127 (2025).
23. David, R., Tuñón, I. & Laage, D. Competing reaction mechanisms of peptide bond formation in water revealed by deep potential molecular dynamics and path sampling. *J. Am. Chem. Soc.* **146**, 14213–14224 (2024).
24. Pavlovic, M., Plucinski, A., Zeininger, L. & Schmidt, B. V. K. J. Temperature sensitive water-in-water emulsions. *Chem. Commun.* **56**, 6814–6817 (2020).

25. Rizzi, G. P. Formation of strecker aldehydes from polyphenol-derived quinones and alpha-amino acids in a nonenzymic model system. *J. Agric. Food Chem.* **54**, 1893–1897 (2006).
26. Shi, Y. et al. The antioxidant mechanism of Maillard reaction products in oil-in-water emulsion system. *Food Hydrocoll.* **87**, 582–592 (2019).
27. Gobert, J. & Glomb, M. A. Degradation of glucose: reinvestigation of reactive α-dicarbonyl compounds. *J. Agric. Food Chem.* **57**, 8591–8597 (2009).
28. Sauer, F. et al. From amino acid mixtures to peptides in liquid sulphur dioxide on early Earth. *Nat. Commun.* **12**, 7182 (2021).
29. Schwendinger, M. G. & &Rode, B. M. Possible role of copper and sodium chloride in prebiotic evolution of peptides. *Anal. Sci.* **5**, 411–414 (1989).

Acknowledgements

This study was financially supported by the Food Quality and Design group in Wageningen University and Research and China Scholarship Council. A part of this study was funded by the National Recovery and Resilience Plan, mission 4, component 2, investment 1.3, call n. 341/2022 of Italian Ministry of University and Research funded by the European Union - NextGenerationEU for the project “ON Foods-Research and innovation network on food and nutrition Sustainability, Safety and Security-Working ON Foods”, project PE00000003, concession decree n. 1550/2022, CUP B83C22004790001.

Author contributions

K.C. prepared the samples, carried out the experiments, curated the data, and wrote the original draft. S.D.P. and A.D.T. performed the HILIC-HRMS analysis and data interpretation. A.M., A.S., and V.F. contributed to the manuscript revision and supervision. All co-authors jointly discussed the results.

Competing interests

The authors declare no competing interests.

Additional information

Supplementary information The online version contains supplementary material available at https://doi.org/10.1038/s42004-026-01951-6.

Correspondence and requests for materials should be addressed to Antonio Dario Troise.

Peer review information Communications Chemistry thanks Nan-Nan Deng and the other, anonymous, reviewer(s) for their contribution to the peer review of this work. A peer review file is available.

Reprints and permissions information is available at http://www.nature.com/reprints

Publisher’s note Springer Nature remains neutral with regard to jurisdictional claims in published maps and institutional affiliations.

Open Access This article is licensed under a Creative Commons Attribution-NonCommercial-NoDerivatives 4.0 International License, which permits any non-commercial use, sharing, distribution and reproduction in any medium or format, as long as you give appropriate credit to the original author(s) and the source, provide a link to the Creative Commons licence, and indicate if you modified the licensed material. You do not have permission under this licence to share adapted material derived from this article or parts of it. The images or other third party material in this article are included in the article’s Creative Commons licence, unless indicated otherwise in a credit line to the material. If material is not included in the article’s Creative Commons licence and your intended use is not permitted by statutory regulation or exceeds the permitted use, you will need to obtain permission directly from the copyright holder. To view a copy of this licence, visit http://creativecommons.org/licenses/by-nc-nd/4.0/.

© The Author(s) 2026